Direct Creation of Finite Element Models from Medical Images using Cartesian Grids

L. Giovannelli, O. Marco, J.M. Navarro, E. Giner, J.J. Ródenas*

Centro de Investigación en Tecnología de Vehículos
Universitat Politècnica de València, Spain

* *Corresponding author. E-mail jjrodena@mcm.upv.es*

ABSTRACT: The aim of this paper is to present an automatic method for creating 2D Finite Element models from medical images based on a hierarchical structure of geometry-independent Cartesian grids (CG-FEM). This strategy provides good quality meshes with a reasonable number of degrees of freedom and reduces the need for previous image segmentation. In addition, with this method, it is possible to include the heterogeneous nature of human tissues in the analysis.

1 INTRODUCTION

The Finite Element Method (FEM) is a numerical technique which allows approximate solutions to be found for problems whose behaviour is described by differential equations, such as the calculation of the displacement and stress fields in a structural component under known boundary conditions. It has become one of the most powerful and widely used tools in the simulation of many types of phenomena and in many fields, above all structural engineering. In the medical field it provides a flexible tool for a number of different applications from the stress analyses of bones to the propagation of tumours. In this area, creating Finite Element (FE) models from medical images and performing patient-specific analyses is a topic of particular interest. In ordinary FE applications the generation of the mesh from CAD models is often one of the most time consuming steps of the whole simulation process, as pointed out by Bishop (2003) and Cottrell et al. (2009). This problem can become challenging in the case of medical images because the surfaces and volumes are not expressed in an explicit form in the first place, but they have to be obtained from bitmaps by means of segmentation tools. It is necessary to avoid the presence of unconnected domains and to make the surfaces close exactly when they define volumes. These problems are not trivial and their solution is hard to automate.

A common approach consists of selecting a number of pixels in the image based on the gray level and assigning an element of the FE mesh to each pixel/voxel, as done for instance by Alberich-Bayarri et al. (2008). This produces hexahedral meshes which, in some cases, can be processed to smooth the external surfaces. This method generates FE models which have a very large number of degrees of freedom and therefore involves a high computational effort. Another common solution is to create surfaces on the basis of the variation of the color levels in the image and to use them to define volumes. Then the unconnected domains have to be deleted and the mesh can finally be created in the usual way as if it were a CAD model, Zhang et al. (2012). In this case, surfaces are required to create perfectly closed volumes, which might possibly need human intervention. The resulting geometry can be seen as extra information which does not exist in the original image.

In both cases the image needs to be heavily processed before mesh tools can be used. Furthermore, the way they deal with material properties usually consists of individuating which living tissue corresponds to each volume and assigning the corresponding material characteristics from literature as if the domains were homogeneous. This makes it impossible to take into account the heterogeneity of the material during the simulation.

On the contrary, in our method the image is meshed directly with a Cartesian grid so that every element contains a number of pixels. Individual material properties are assigned to each pixel on the basis of its own gray scale value. Then, all the pixels are used for the evaluation of the element matrices so that an homogenization of the material properties is performed at the element level. In this way, the boundaries remain implicit and are expressed only in the variation of the material properties in each element. To reduce the inaccuracy due to the homogenization process, a mesh

refinement is performed guided by statistical magnitudes of the pixel values in every element. The result is that the mesh is finer where the image is more heterogeneous and coarser where it is more homogeneous.

Our method lightens the segmentation step: the only geometric entities that must be explicitly defined are the areas where the boundary conditions have to be imposed. In addition this strategy allows *h*-adaptive refinement to be performed in a fast and simple way.

Even if the application of this method to 2D images is of limited interest from the clinical point of view, nonetheless it represents an essential preliminary step before moving to 3D simulations with CT series. In this case, the Hounsfield scale, used in CT scans, is more suitable for our purpose since it is an absolute scale and has better capability of distinguishing different materials.
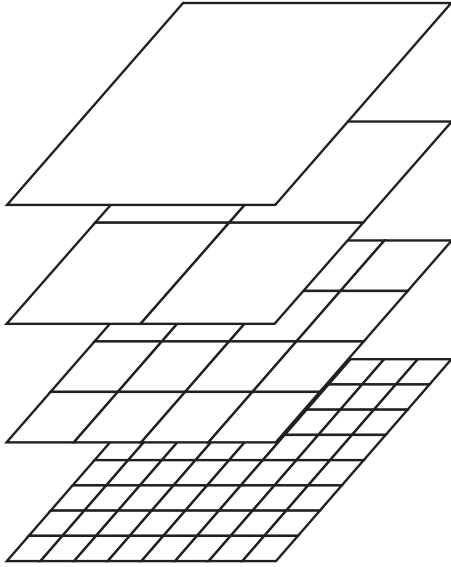

Figure 1: Hierarchical structure of nested Cartesian grids

2 METHODOLOGY

Creating the FE model means, in the first place, calculating the global stiffness $\mathbf{K}$ matrix which describes the elastic behaviour of the system. Afterwards the boundary conditions will be imposed and the problem will be solved. The stiffness matrix $\mathbf{K}$ is obtained by assembling the stiffness matrices $\mathbf{k^e}$ of the elements of the mesh. Equation 1 shows the numerical integration necessary to calculate the matrix $\mathbf{k^e}$.

$$
\begin{aligned}
\mathbf{k^e} &= \int_{A^e} \mathbf{B^T D B} dA = \\
&= \sum_{i=1}^{IP} \mathbf{B}^T(\xi_i, \eta_i) \mathbf{D}(\xi_i, \eta_i)) \mathbf{B}(\xi_i, \eta_i) \mid \mathbf{J}(\xi_i, \eta_i) \mid w_i
\end{aligned}
$$

(1)

In which IP represents the number of integration points, (ξ_i, η_i) their positions in the element local coordinates, $\mid \mathbf{J}(\xi_i, \eta_i) \mid$ the corresponding Jacobian determinant and w_i the weights associated to the integration points depending on the quadrature rule chosen.

In our technique we will use the numerical integration process to include the different material properties assigning one integration point to each pixel. To do this, a quadrature rule based on the Riemann sum is performed instead of the more common Gauss-Legendre quadrature. Therefore the integration points lie on the centres of the pixels and the weights w_i correspond to the pixel areas in local coordinates, as will be shown later in Figure 3. In practice, the model creation process can be divided into a number of steps. Each of them is shown in detail in the following:

- introduction of the bitmap into the hierarchical structure of Cartesian grids

- creation of the $\mathbf{B}$ matrices which consider the geometry of each of the finite elements used in the analysis.

- creation of the $\mathbf{D}$ matrices which describe the material behaviour at each point.

- element integration

- enforcement of the boundary conditions

2.1 *The nested Cartesian grid structure*

The core of the method is the use of a structure of nested Cartesian grids for the creation of the FE mesh, Nadal et al. (2013). The first level grid is created by dividing in four regular elements a square in a parametric space. Each new level is obtained by dividing in four the elements of the previous level, as can be seen in Figure 1, in which the lowest mesh levels are shown. This means that the generic level n contains $2^n \times 2^n$ elements. The elements of these grids, their topology and connectivity, are not stored; they exist thanks to a number of routines which can easily calculate them because of the hierarchical structure of the Cartesian grids. The space of the Cartesian structure is then related with the space of the image. This solution allows the calculation mesh to be created or changed very fast and needs small amounts of information storage.

In the first place, the pixels are structured in an initial mesh, which can correspond to the Cartesian grid of a certain level, Figure 2. Then a group of pixels will be assigned to each element, see Figure 3. Then elements outside the area of interest can be ignored and the mesh is refined guided by the distribution of the grey level values in each element. The result is a structured non-conforming mesh, Figure 4, in which, at the border between elements belonging to different levels there are so-called hanging nodes: nodes
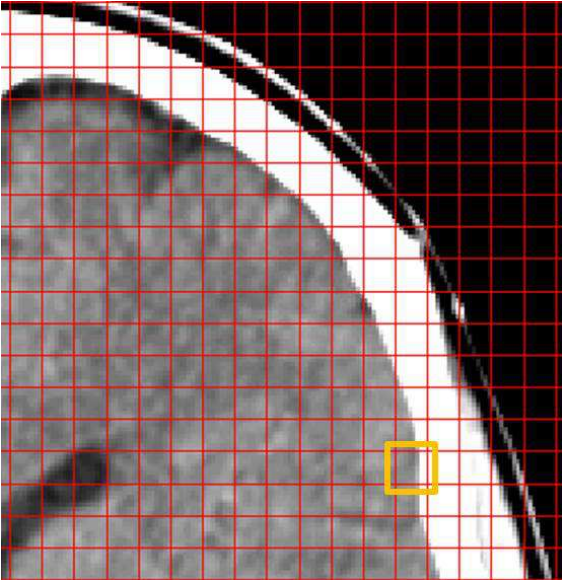
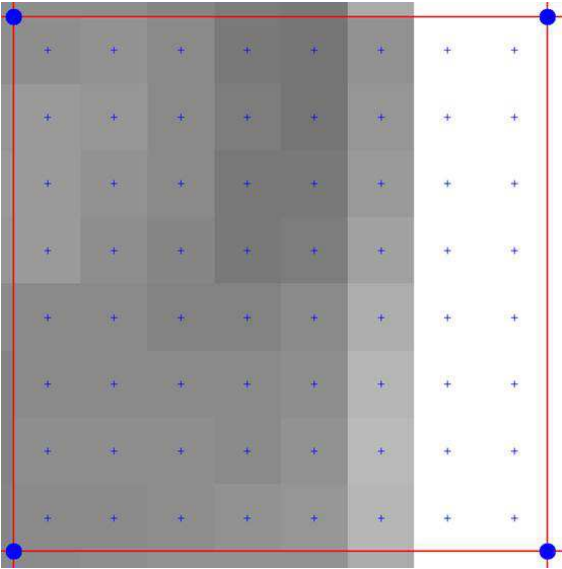Figure 2: Head CT cross-section structured into uniform CG-FEM mesh

Figure 3: Detail of an element from Figure 2. The integration points are represented as blue crosses

which belong to the smaller element but not to the bigger one even if they lie on its contour. These are subjected to multi-point constraints in order to guarantee the C^0 continuity of the displacement field. The refinement is performed substituting an element (parent) with its four children in the next refinement level. The surrounding elements (neighbours) are refined if the difference of level of the contacting elements becomes greater than one. Three criteria have been implemented for the choice of the elements to refine; they are based on the evaluation of different statistical magnitudes of the grey scale values in each element. These criteria are respectively dependent on the calculation of:

- the mean and median values of the pixels

- the range of the pixels values
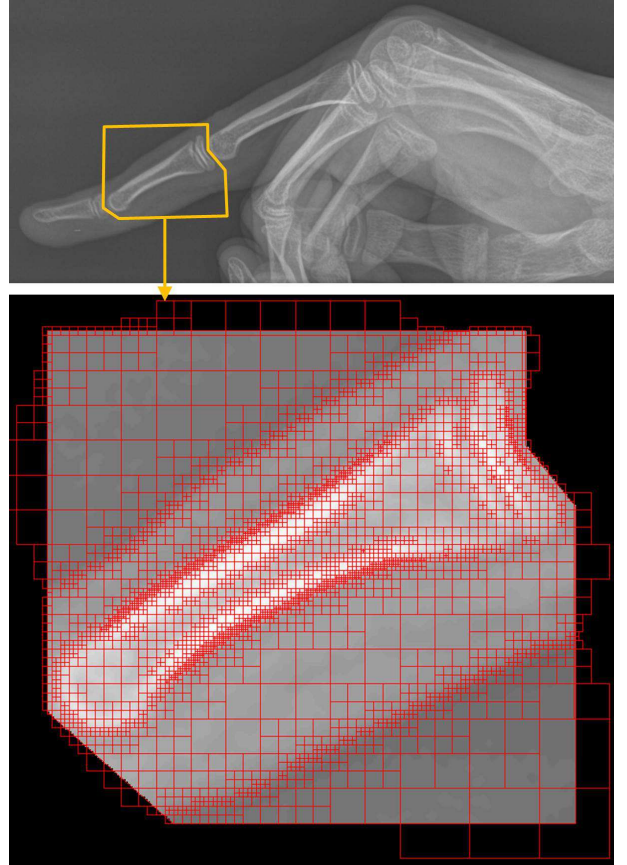
- the mean value and standard deviation

Figure 4: H-refined mesh of a detail from the radiography of a hand

In order to guarantee the possibility of performing the refinement until the mesh level contains only one pixel per element, it is mandatory that the image dimensions, measured in pixels, are powers of two. Since, in general, this does not happen, additional pixels are added to the image when it is read in order to fulfil this condition. These additional pixels are given the grey scale value corresponding to null material properties.

2.2 *Efficient calculation of the B matrix*

In the FE solution of the elasticity problem, in every element, the relation between strains ε_e and nodal displacements $\mathbf{u_e}$ is expressed by the $\mathbf{B}$ matrix (Equation 2), necessary for the integration of Equation 1.

$$\varepsilon_e = \mathbf{Bu_e} \qquad (2)$$

In particular, it is necessary to calculate the values of the $\mathbf{B}$ matrix at the integration points of each element. Here, the integration points are chosen to lie on the centres of the pixels contained in the mesh. Hence, for elements belonging to the same mesh level, the number of the integration points and their position in local coordinates are identical and, in addition, the elements share the same shape and size. Obviously the same occurs for the $\mathbf{B}$ matrix therefore it can be calculated in advance and stored for each level used in the calculation mesh whereas in a usual FE mesh the $\mathbf{B}$ matrix has to be calculated for every single element.

2.3 Material properties

One of the most important assumptions of this method is that a univocal relation can be created between material properties and pixel values. A number of papers have proposed relations between Hounsfield values in CT scans and mechanical properties of human bones such as Rho et al. (1995), Gupta & Dan (2004). Since in this paper we are at a preliminary stage, the usual grey scale has been used instead of the Hounsfield units for simplicity. When the material properties are given to the software, the grey level they refer to is specified and an automatic linear interpolation is performed to complete the assignation of material properties to each value of the grey scale. In particular, the interpolated magnitudes can be the matrix **D**, which relates strain and stress, or the engineering elastic constants used for its calculation.

The resulting dependence of the generic material property on the pixel values is similar to the one shown in Figure 5.
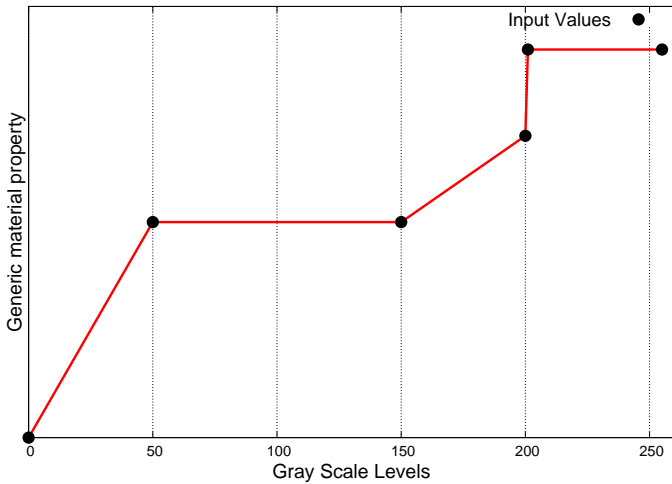

Figure 5: Representation of general material property assignation to the grey scale values of the pixels

2.4 Element integration

Once the material properties are available at the centres of the pixels and the **B** matrix has been evaluated for each integration point, the element stiffness matrix $\mathbf{k}_e$ can be evaluated using (1).

2.5 Enforcement of the boundary conditions

In the simulation process the only geometric entities required are those used to enforce the Dirichlet and Neumann boundary conditions. In this work, they are generated manually by the user who has to define the points used to interpolate a NURBS that will define the surface where the boundary conditions will be applied. In general, the nodes of the FE model do not lie on these curves, therefore the imposition of the Dirichlet conditions cannot be enforced directly on the nodes. Instead it is performed by using a mortar method similar to the one used by Moës et al. (2006).

Regarding the Neumann conditions, they only require the evaluation of the integrals along internal boundaries in the elements.

3 NUMERICAL RESULTS

In the following paragraphs two numerical examples are presented. The first one is a study of the convergence rate of the FE solution and is meant to test the method from the numerical point of view. In the second one a stress analysis of the x-ray image of a femur is performed. This last result is mainly meant to be a test to check the method with an actual medical image, it does not model any real problem, because of the dimension (the clinical applications of interest are mainly 3D) and because of the limited capability of 2D conventional x-ray scans to characterize the human tissues, due both to the influence of the third dimension on the values of the pixels and the limitations of the standard gray scale. The fact that the results are plausible (for a 2D problem) makes the application of the method to CT scans in the 3D space very promising.

3.1 Validation

For the validation of the proposed method, the 2D problem of a tube with circular cross-section under internal pressure has been analysed with the hypothesis of plain strain condition. Firstly the problem has been modelled by exactly representing the boundary with straight lines and NURBS (see Figure 6 and table 1) and in the second place bitmaps of different resolution have been taken from it (Figure 7).
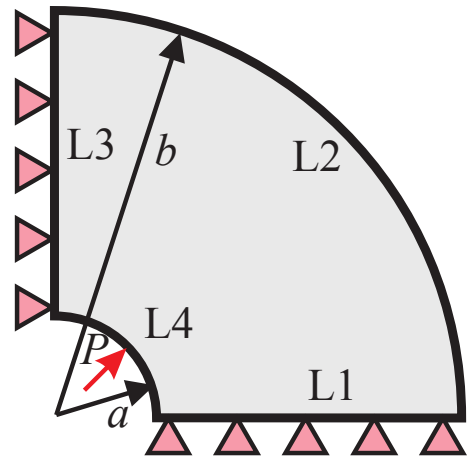

Figure 6: One forth of pipe section with internal pressure in plain strain condition, extracted from Nadal et al. (2013).

a [m]	3
b [m]	6
P [MPa]	1

Table 1: Geometric characteristics and load referred to image 6.

The different models have been meshed with uniform meshes of different levels and solved. The geo-

metric one by using a standard CG-FEM solver and the images by using the method proposed in this paper. In Table 2 the material properties introduced for the black (Gray Scale 0) and white (Gray Scale 255) pixels respectively are shown. The material properties for the intermediate gray levels have been calculated by linear interpolation. For the geometric case, the values of the Material 2 (table 2) have been used for the closed domain as it is done for the white pixels of the image.
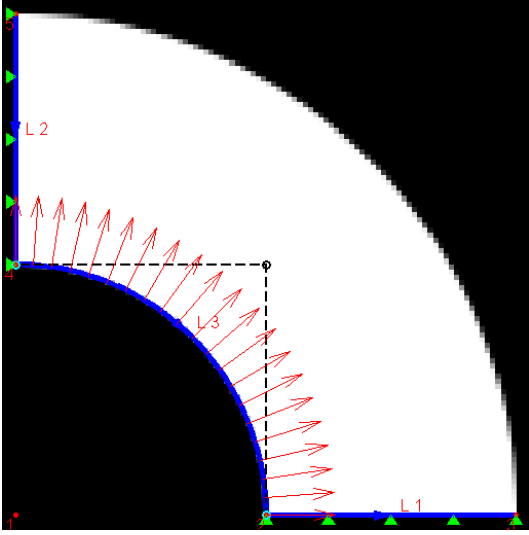

Figure 7: Tube under pressure defined by a bitmap representing the geometrical model (Figure 6), with boundary conditions imposed upon.

Material	E [MPa]	ν	Gray level
Material 1	0	0.0	0
Material 2	1000	0.3	255

Table 2: Material Properties used for the convergence study.

Figure 8 shows the evolution of the error in energy norm for the geometric case and images with different resolution when the number of degrees of freedom increases (i.e. for increasingly refined meshes). The spatial resolutions of the bitmaps are 3.25, 13 and 52 pixels per inch. The error in energy norm is expressed in equation 3, where σ represents the exact stress field, σ^h represents the stress field of the FE solution, $\mathbf{D}$ is the Hooks tensor, and Ω the meshed domain.

$$||\mathbf{e}||^2 = \frac{1}{2}\int_\Omega (\sigma - \sigma^h)^T \mathbf{D}^{-1}(\sigma - \sigma^h)^T d\Omega \qquad (3)$$

As shown in Figure 8 the convergence curves of the different problems are similar. As expected, the error in energy norm gets closer to the geometric case, as the image resolution increases. This corresponds to the increasingly better approximation of the image to the exact geometry, defined by NURBS, as its spatial resolution is enhanced. As the number of degrees of freedom increases the curves get separated. This is due to the fact that the refinement of the mesh makes the FE solution closer to the exact solution but the
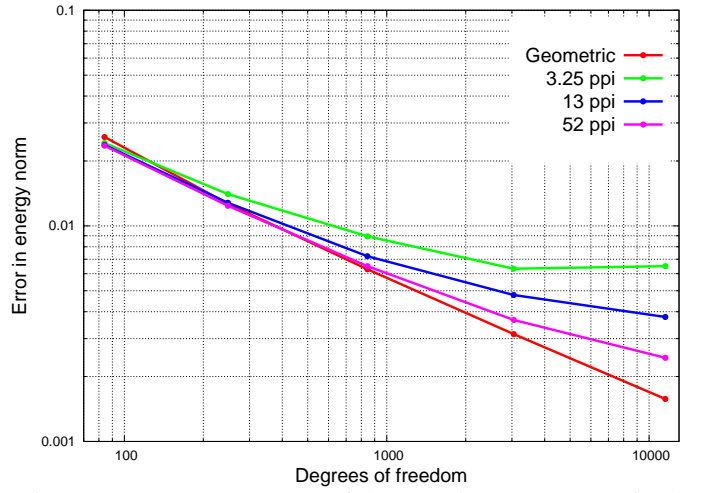

Figure 8: Convergence rates of the error in energy norm for the geometric problem and the bitmaps.

exact geometry corresponding to the bitmaps is different from the geometric representation of the tube and each image converges to its own exact solution.

3.2 *Long bone mechanical analysis*

Finally, our method has been applied to the x-ray of a femur in order to create a 2D FE model and to perform the calculation of the stress induced by a load distributed on the joint. The area of interest of the x-ray was selected, a NURBS was used to define an arc on the femur joint and a parabolic symmetric pressure, with maximum value of 10 MPa and 0 MPa at the arc edges. Furthermore, a straight line was added at the bottom of the image and the problem was given homogeneous Dirichlet boundary conditions on it by using Lagrange multipliers. The FE mesh was created performing an *h*-refinement on a coarse uniform mesh of level 2. To do this the maximum refinement level allowed was 9 and the maximum value of the ratio between standard deviation and mean gray scale value at the pixels was set to 3 in each element. Figure 9 shows the x-ray image of a femur and its corresponding *h*-adapted FE model.

The material properties used for this simulation have been taken from literature, (Viceconti et al. 1998) and (Kim et al. 2010), and are shown in table 3 together with the associated gray levels.

Material	E [GPa]	ν	Gray level
Bone	14.200	0.30	255
Muscle	0.645	0.43	150
Air	0.000	0.00	0

Table 3: Material Properties referred to Figure 9.

The Von Mises stress field calculated at the integration points is shown in Figure 10. The stress distribution is clearly the expected one for a compression-bending problem with higher values of the stress in the lower part of the image. In this area the maximum stress values correspond to the zones were the cortical bone appears to be thicker (in the 2D problem).

The result is quite in accordance with the functional structure of the long bones, despite the fact that 2D x-ray give information polluted by the effect of the third dimension and the gray scale is not reliable for the tissue recognition.
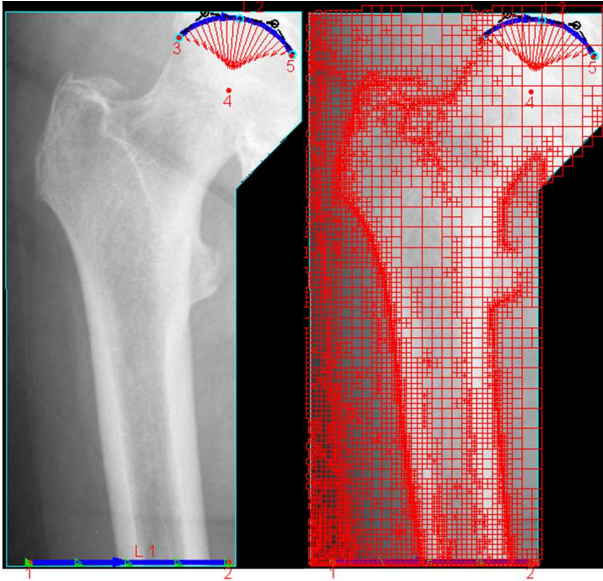

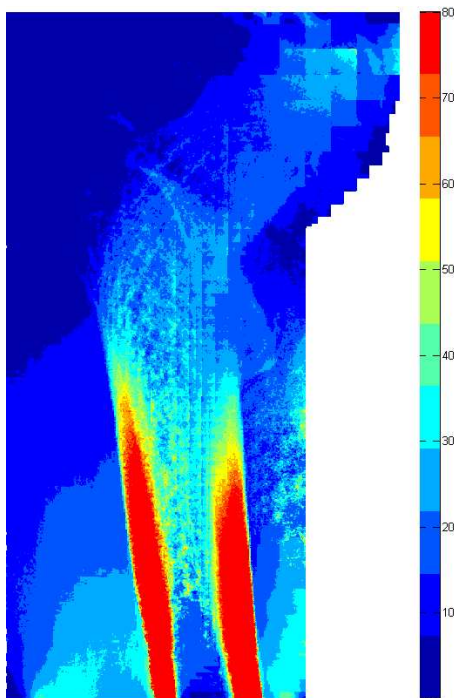Figure 9: X-ray image of a femur and *h*-adapted FE model.

Figure 10: Von Mises Stress Field of femur.

4 CONCLUSIONS

A method for direct creation of FE models from medical images has been proposed, based on a hierarchical structure of nested Cartesian grids. It is capable of creating and of refining FE models with a little user intervention and taking into account the heterogeneity of the human tissues provided that a reliable correlation between pixel values and material properties is available. The comparison between the FE model obtained by a geometric problem and the models created from its images at different resolutions shows good convergence rates. In the case of the image-based FE models the error in energy norm is affected not only by the element dimension but also by the resolution of the image, as expected. Furthermore the 2D simulation of a femur under distributed pressure gave reasonable results. The numerical results are very promising about the potentiality of the method for the creation of 3D models from CT-scans which will enable us to assign properties rigorously and to get closer to the real behaviour of human tissues.

REFERENCES

Alberich-Bayarri, A., L. Marti-Bonmati, R. Sanz-Requena, E. Belloch, & D. Moratal (2008). In vivo trabecular bone morphologic and mechanical relationship using high-resolution 3-t mri. *American Journal of Roentgenology 191*, 721–726.

Bishop, J. (2003). Rapid stress analysis of geometrically complex domains using implicit meshing. *Computational Mechanics 30*, 460–478.

Cottrell, J., T. Hughes, & Y. Bazilevs (2009). *Isogeometric Analysis: Toward Integration of CAD and FEA*. Wiley.

Gupta, S. & P. Dan (2004). Bone geometry and mechanical properties of the human scapula using computed tomography data. *Trends in Biomaterials & Artificial Organs 17*, 61–70.

Kim, H., P. Jürgens, S. Weber, L. Nolte, & M. Reyes (2010). A new soft-tissue simulation strategy for cranio-maxillofacial surgery using facial muscle template model. *Progress in Biophysics and Molecular Biology 103*, 284–291.

Moës, N., E. Béchet, & M. Tourbier (2006). Imposing dirichlet boundary conditions in the extended finite element method. *International Journal for Numerical Methods in Engineering 67*, 1641–1669.

Nadal, E., J. Ródenas, J. Albelda, M. Tur, J. Tarancón, & F. Fuenmayor (2013). Efficient finite element methodology based on cartesian grids: Application to structural shape optimization. *Abstract and Applied Analysis 2013*, Article ID 953786, 19 pages.

Rho, J., M. Hobatho, & R. Ashman (1995). Relations of mechanical properties to density and ct numbers in human bone. *Medical Engineering & Physics 17*, 347–355.

Viceconti, M., L. Bellingeri, L. Cristofolini, & A. Toni (1998). A comparative study on different methods of automatic mesh generation of human femurs. *Medical engineering & physics 20*, 1–10.

Zhang, J., D. Malcolm, J. Hislop-Jambrich, C. Thomas, & P. Nielsen (2012). Automatic meshing of femur cortical surfaces from clinical ct images. *Lecture Notes in Computer Science 7599*, 40–48.